Supplemental Material to "High-throughput computation of Raman spectra from first principles"

Mohammad Bagheri[1] **and Hannu-Pekka Komsa**[1,*]

[1]Microelectronics Research Unit, Faculty of Information Technology and Electrical Engineering, University of Oulu, Oulu, FIN-90014, Finland
[*]corresponding author(s): Hannu-Pekka Komsa (hannu-pekka.komsa@oulu.fi)

Contents

List of Tables

List of Figures

Benchmark

To benchmark of our approach, we selected four materials with different band gaps and different atomic masses: Si, PbO, AlN, and $Cd(HO)_2$. We first verified that the standard approach of calculating Raman-tensors for all modes agrees with the Raman-active modes identified using group theory. That is, all the Raman-inactive modes were found to have vanishingly small Raman tensor, although often nonzero due to numerical errors.

Next, we investigated the effect of k-point mesh density on Raman tensors and Raman spectra. We calculated Raman tensors for R_k = 30, 40 and 60 and compared the results with the standard value (R_k = 20) used in Phonon database. Results from two (out of four) materials are shown in Fig. S1, where, to represent large and small bandgap materials, we selected AlN (4.05 eV) and Si (0.85 eV), respectively. Fig. S1(a,b) shows the unnormalized Raman activity spectra for different R_k, which clearly illustrates that AlN is hardly affected whereas Si experiences significant changes, thus suggesting that R_k should be increased. To better illustrate the magnitude of changes, Fig. S1(c,d) show how the maximum intensity changes with increasing R_k and Fig. S1(e,f) shows the average dielectric constant. In the case of AlN, R_k = 20 already yields Raman tensors within 10 % of the converged value and dielectric constant within 1 %. In the case of Si, R_k = 40 is required to reach similar accuracy. Based on these results we

decided to use R_k=40 for materials with bandgap smaller than 1 eV, R_k=30 for materials with bandgap between 1 eV to 2 eV, and R_k=20 for materials with a bandgap greater than 2 eV.

In the third step, we investigated the effect of step size by calculating Raman tensors of PbO and $Cd(HO)_2$ with step sizes of 0.001, 0.02, and 0.04 Å and compared them with those using the standard step size of 0.005 Å. Fig. S2 shows the changes in dielectric constants of PbO and $Cd(HO)_2$ in different directions and plotted for three-step sizes: 0.005, 0.02, and 0.04 Å. Since dielectric tensor is symmetric (xy=yx, xz=zx, and yz=zy), we only plot the inequivalent components. As shown in Fig. S2, whenever there are pronounced changes in the dielectric constant (corresponding to non-zero components in Raman tensor), the dependence on step size is close to linear. In some cases there is a small parabolic dependence, seen particularly well in the xy=yx component which contains no linear dependence, but these will not affect the Raman tensor since we are using two-point finite-difference stencil. Moreover, in this range of step sizes there is no discernible noise, although some noise could be observed in 0.001 Å results (not shown). Thus, we consider the default value of 0.005 Å a good choice.

As mentioned in the text, there was an error in the normalization of eigenvectors in Atomate. We fixed the normalization error and changed the formulations to match with the vasp_raman code[1,2]. To verify our approach, we used vasp_raman code to calculate Raman tensors and compared them to Atomate with the fixed and old versions of eigenvector normalization. Fig. S3 shows the Raman activity spectra of MoS_2, WS_2, SrGaSnH, and BaAlSiH. The revised normalization yields activities closely matching with vasp_raman code. The incorrect normalization, on the other hand, tends to lead to overestimation of Raman activities and is particularly severe with modes that have very small Raman activity.

In CRD website (https://ramandb.oulu.fi), the total Raman intensity is separated into depolarized ($I_\perp$) and polarized ($I_{||}$) components, $I = I_\perp + I_{||}$, with

$$\frac{I_{||}}{(\omega_L - \omega_\nu)^4} \sim \frac{\hbar(n+1)}{30\omega_\nu}(10G_\nu^{(0)} + 4G_\nu^{(2)}) \tag{1}$$

$$\frac{I_\perp}{(\omega_L - \omega_\nu)^4} \sim \frac{\hbar(n+1)}{30\omega_\nu}(5G_\nu^{(1)} + 3G_\nu^{(2)}) \tag{2}$$

where we have taken out the $(\omega_L - \omega_\nu)^4$ term that depends on the laser wavelength, since (i) this removes the dependence on one external parameter from our spectra, (ii) our calculations are for non-resonant conditions and one needs to be careful to only compare to wavelengths that are far from resonance, and (iii) the dependence on ω_ν and thus the changes in the spectra after normalization are usually small. The rotation invariants are[3,4]

$$G_\nu^{(0)} = \frac{1}{3}(R_{\nu xx} + R_{\nu yy} + R_{\nu zz})^2 \tag{3}$$

$$G_\nu^{(1)} = \frac{1}{2}[(R_{\nu xy} - R_{\nu yx})^2 + (R_{\nu xz} - R_{\nu zx})^2 + (R_{\nu zy} - R_{\nu yz})^2] \tag{4}$$

$$G_\nu^{(2)} = \frac{1}{2}[(R_{\nu xy} + R_{\nu yx})^2 + (R_{\nu xz} + R_{\nu zx})^2 + (R_{\nu zy} + R_{\nu yz})^2] + \frac{1}{3}[(R_{\nu xx} - R_{\nu yy})^2 + (R_{\nu xx} - R_{\nu zz})^2 + (R_{\nu zz} - R_{\nu yy})^2] \tag{5}$$

Mineral name	Formula	mpid	Energy above hull (eV)	RRUFF ID
Billingsleyite	Ag_7AsS_6	mp-15077	0.003	**R070350**
Sanbornite	$BaSi_2O_5$	mp-3031	0	**R060489**
Hardystonite	$Ca_2ZnSi_2O_7$	mp-6227	0.015	**R040026**
Perovskite	$CaTiO_3$	mp-4019	0	**R050456**
Greenockite	CdS	mp-672	0	**R090045**
Cobaltite	CoAsS	mp-4627	0.001	**R070372**
Cobaltite	CoAsS	mp-16363	0.004	**R060907**
Cuprite	Cu_2O	mp-361	0	**R050374**
Stromeyerite	CuAgS	mp-5014	0.024	**R060908**
Emplectite	$CuBiS_2$	mp-22982	0	**R070307**

Continued on next page

Table S1 – continued from previous page

Mineral name	Formula	mpid	Energy above hull (eV)	RRUFF ID
Chalcostibite	$CuSbS_2$	mp-4468	0	**R060262**
Pyrite	FeS_2	mp-226	0.008	**R050070**
Marcasite	FeS_2	mp-1522	0	**R060882**
Langbeinite	$K_2Mg_2(SO_4)_3$	mp-6299	0	**R070285**
Aphthitalite	$K_3Na(SO_4)_2$	mp-22457	0	**R050651**
Goldschmidtite	$KNbO_3$	mp-7375	0	**R190009**
Nordite-(La)	$Na_3SrLaZnSi_6O_{17}$	mp-13726	0	**R140310**
Swedenborgite	$NaBe_4SbO_7$	mp-8075	0	**R060486**
Leucophanite	$NaCaBeSi_2O_6F$	mp-560721	0	**R050004**
Neighborite	$NaMgF_3$	mp-2955	0	**R080108**
Cotunnite	$PbCl_2$	mp-23291	0.006	**R060655**
Matlockite	PbClF	mp-22964	0	**R140538**
Laurite	RuS_2	mp-2030	0	**R110120**
Zincite	ZnO	mp-2133	0	**R060027**
Chrysoberyl	$BeAl_2O_4$	mp-3081	0	**R040073**
Wurtzite	ZnS	mp-10281	0.002	**R130069**
Montroydite	HgO	mp-1224	0	**R070235**
Quartz	SiO_2	mp-7000	0.011	**R050125**
Bromellite	BeO	mp-2542	0	X050194
Litharge	PbO	mp-19921	0.001	R060959
Romarchite	SnO	mp-2097	0	R080006
Anatase	TiO_2	mp-390	0.006	R060277
Andalusite	Al_2SiO_5	mp-4753	0	R050258
Anglesite	$Pb(SO_4)$	mp-3472	0	R040004
Aragonite	$CaCO_3$	mp-4626	0.024	R040078
Baryte	$Ba(SO_4)$	mp-3164	0	R040036
Brenkite	$Ca_2CO_3F_2$	mp-6246	0.028	R060247
Calcite	$CaCO_3$	mp-3953	0	R040070
Cerussite	$Pb(CO_3)$	mp-19893	0	R040069
Colquiriite	$CaLiAlF_6$	mp-1224	0	R070417
Dolomite	$CaMg(CO_3)_2$	mp-6459	0	R050129
Eitelite	$Na2Mg(CO_3)_2$	mp-6026	0	R110214
Eulytine	$Bi_4(SiO_4)_3$	mp-23331	0	R060058
Farringtonite	$Mg_3(PO_4)_2$	mp-14396	0	R130127
Geikielite	$MgTiO_3$	mp-3771	0	R070479
Glauberite	$Na_2Ca(SO_4)_2$	mp-6397	0	R050350
Huntite	$CaMg_3(CO_3)_4$	mp-6524	0.004	R040126
Cristobalite	SiO_2	mp-6945	0.003	R070235
Leiteite	$ZnAs_2O_4$	mp-29509	0.006	R040011
Lithiophosphate	$Li_3(PO_4)$	mp-2878	0.001	R100092
Magnesite	$Mg(CO_3)$	mp-5348	0	R040114
Nahcolite	$NaH(CO_3)$	mp-696396	0	R070237
Witherite	$Ba(CO_3)$	mp-5504	0	R040040
Arsenolite	As_2O_3	mp-2184	0.009	R050383
Åkermanite	$Ca_2MgSi_2O_7$	mp-6094	0.023	R061085
Benitoite	$BaTi(SiO_3)_3$	mp-6661	0	R050320
Gahnite	$ZnAl_2O_4$	mp-2908	0	R070591
Rosiaite	$PbSb_2O_6$	mp-20727	0	R070384
Xanthoconite	Ag_3AsS_3	mp-561620	0	R070746
Topaz	$Al_2SiO_4F_2$	mp-6280	0	R040121

Continued on next page

Table S1 – continued from previous page

Mineral name	Formula	mpid	Energy above hull (eV)	RRUFF ID
Imiterite	Ag_2HgS_2	mp-9635	0.03	R080014
Acanthite	Ag_2S	mp-610517	0.024	R070578
Argyrodite	Ag_8GeS_6	mp-9770	0	R050437
Andalusite	Al_2SiO_5	mp-4934	0.007	R050258
Nitrobarite	$Ba(NO_3)_2$	mp-4396	0	R060622
Barylite	$BaBe_2Si_2O_7$	mp-6383	0	R060620
Barylite	$BaBe_2Si_2O_7$	mp-12797	0	R060606
Guanajuatite	Bi_2Se_3	mp-23164	0.028	R080140
Merwinite	$Ca_3Mg(SiO_4)_2$	mp-558209	0.038	R070195
Rankinite	$Ca_3Si_2O_7$	mp-3932	0.009	R140775
Hurlbutite	$CaBe_2(PO_4)_2$	mp-6772	0	R090048
Rynersonite	$CaTa_2O_6$	mp-18229	0	R080064
Arsenopyrite	FeAsS	mp-561511	0	R050071
Gudmundite	FeSbS	mp-27904	0	R060741
Cinnabar	HgS	mp-634	0.004	R070532
Cinnabar	HgS	mp-9252	0.004	R070532
Kalsilite	$KAlSiO_4$	mp-8355	0.002	R060801
Kalsilite	$KAlSiO_4$	mp-9480	0.002	R060030
Avogadrite	KBF_4	mp-4929	0	R110062
Kotoite	$Mg_3(BO_3)_2$	mp-5005	0	R060940
Natrosilite	$Na_2Si_2O_5$	mp-3193	0	R060855
Molybdomenite	$PbSeO_3$	mp-20716	0	R140388
Valentinite	Sb_2O_3	mp-2136	0	R120096
Stibnite	Sb_2S_3	mp-2809	0	R120137
Moissanite	SiC	mp-7631	0	R150016
Tellurite	TeO_2	mp-2125	0	R070606
Rutile	TiO_2	mp-2657	0.037	R060745, R120008
Brookite	TiO_2	mp-1840	0.02	R050363, R050591, R130225
Lorándite	$TlAsS_2$	mp-4988	0	R110055
Tungstenite	WS_2	mp-224	0	R070616
Waimirite-(Y)	YF_3	mp-2416	0	R130714
Reinerite	$Zn_3(AsO_3)_2$	mp-27580	0	R080132
Baddeleyite	ZrO_2	mp-2858	0	R100171

Table S1. Common structures in our database based on the same chemical formula and the mineral name in RRUFF compared to Materials Project tags. The bold RRUFF IDs refer to structures that have also similar lattice parameters.

Point group	Irrep. label	Raman Activity	Point group	Irrep. label	Raman Activity
C_1(1)	A	True	C_6 (6)	A	True
C_i(-1)	A_g	True		B	False
	A_u	False		E_1	True
C_2 (2)	A	True		E_2	True
	B	True	C_{3h} (-6)	A′	True
$C_{1v} = C_s = C_{1h}$ (m)	A′	True		E′	True
	A″	True		A″	False
C_{2h} (2/m)	A_g	True		E″	True
	B_g	True	C_{6h} (6/m)	A_g	True
	A_u	False		B_g	False
	B_u	False		E_{1g}	True

Continued on next page

Table S2 – continued from previous page

Point group	Irrep. label	Raman Activity	Point group	Irrep. label	Raman Activity
D_2 (222)	A	True		E_{2g}	True
	B_1	True		A_u	False
	B_2	True		B_u	False
	B_3	True		E_{1u}	False
C_{2v} (mm2)	A_1	True		E_{2u}	False
	A_2	True	D_6 (622)	A_1	True
	B_1	True		A_2	False
	B_2	True		B_1	False
D_{2h} (mmm)	A_g	True		B_2	False
	B_{1g}	True		E_1	True
	B_{2g}	True		E_2	True
	B_{3g}	True	C_{6v} (6mm)	A_1	True
	A_u	False		A_2	False
	B_{1u}	False		B_1	False
	B_{2u}	False		B_2	False
	B_{3u}	False		E_1	True
C_4 (4)	A	True		E_2	True
	B	True	D_{3h} (-6m2)	A'_1	True
	E	True		A'_2	False
S_4 (-4)	A	True		E′	True
	B	True		A''_1	False
	E	True		A''_2	False
C_{4h} (4/m)	A_g	True		E″	True
	B_g	True	D_{6h} (6/mmm)	A_{1g}	True
	E_g	True		A_{2g}	False
	A_u	False		B_{1g}	False
	B_u	False		B_{2g}	False
	E_u	False		E_{1g}	True
D_4 (422)	A_1	True		E_{2g}	True
	A_2	False		A_{1u}	False
	B_1	True		A_{2u}	False
	B_2	True		B_{1u}	False
	E	True		B_{2u}	False
C_{4v} (4mm)	A_1	True		E_{1u}	False
	A_2	False		E_{2u}	False
	B_1	True	T (23)	A	True
	B_2	True		E	True
	E	True		T	True
D_{2d} (-42m)	A_1	True	T_h (m-3)	A_g	True
	A_2	False		A_u	False
	B_1	True		E_g	True
	B_2	True		E_u	False
	E	True		T_g	True
D_{4h} (4/mmm)	A_{1g}	True		T_u	False
	A_{2g}	False	O (432)	A_1	True
	B_{1g}	True		A_2	False
	B_{2g}	True		E	True
	E_g	True		T_1	False
	A_{1u}	False		T_2	True
	A_{2u}	False	T_d (-43m)	A_1	True
	B_{1u}	False		A_2	False
	B_{2u}	False		E	True

Continued on next page

Table S2 – continued from previous page

Point group	Irrep. label	Raman Activity	Point group	Irrep. label	Raman Activity
	E_u	False		T_1	False
C_3 (3)	A	True		T_2	True
	E	True	O_h (m-3m)	A_{1g}	True
S_6 (-3)	A_g	True		A_{2g}	False
	E_g	True		E_g	True
	A_u	False		T_{1g}	False
	E_u	False		T_{2g}	True
D_3 (32)	A_1	True		A_{1u}	False
	A_2	False		A_{2u}	False
	E	True		E_u	False
C_{3v} (3m)	A_1	True		T_{1u}	False
	A_2	False		T_{2u}	False
	E	True			
D_{3d} (-3m)	A_{1g}	True			
	A_{2g}	False			
	E_g	True			
	A_{1u}	False			
	A_{2u}	False			
	E_u	False			

Table S2. Raman activity of all point groups and irreducible representation (irrep.) based on group theory. True means active and False means inactive

Formula	Avg[$\Delta\omega$] (cm^{-1})	Avg[ΔI] (a.u.)	Std(Freq) (cm^{-1})	Std(I) (a.u.)
HgO	3.52	-0.02	11.35	0.02
SiO_2	18.54	-0.02	5.95	0.03
$MgCO_3$	6.67	-0.05	12.26	0.07
$CaMg(CO_3)_2$	2.61	0.04	14.78	0.15

Table S3. Comparison of calculated frequencies and intensities with those obtained from the fits to the experimental spectra shown in Figure 5. Frequency and intensity differences are defined as $\Delta\omega = \omega_{\text{fit}} - \omega_{\text{calc}}$ and $\Delta I = I_{\text{fit}} - I_{\text{calc}}$, where I is the normalized intensity. Std refers to standard deviation.

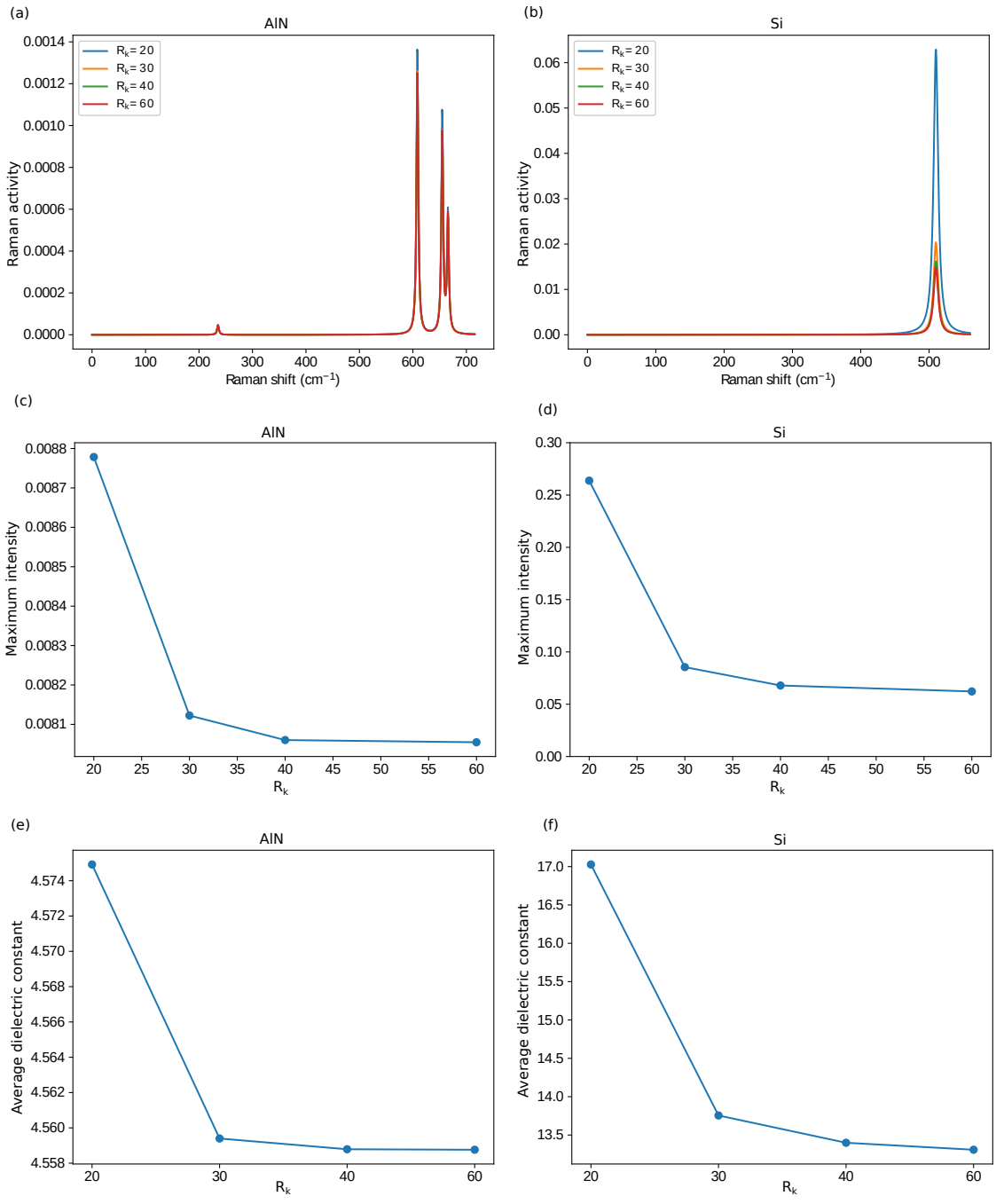

Figure S1. The effect of k-point mesh parameter R_k. (a) and (b) show the unnormalized Raman activity of AlN and Si, respectively, with R_k = 20 (blue line), 30 (orange line), 40 (green line) and 60 (red line). (c) and (d) show the effects of different R_k on the maximum intensity of AlN and Si spectra, respectively. (e) and (f) show the effects of different R_k on the average dielectric constant of AlN and Si, respectively.

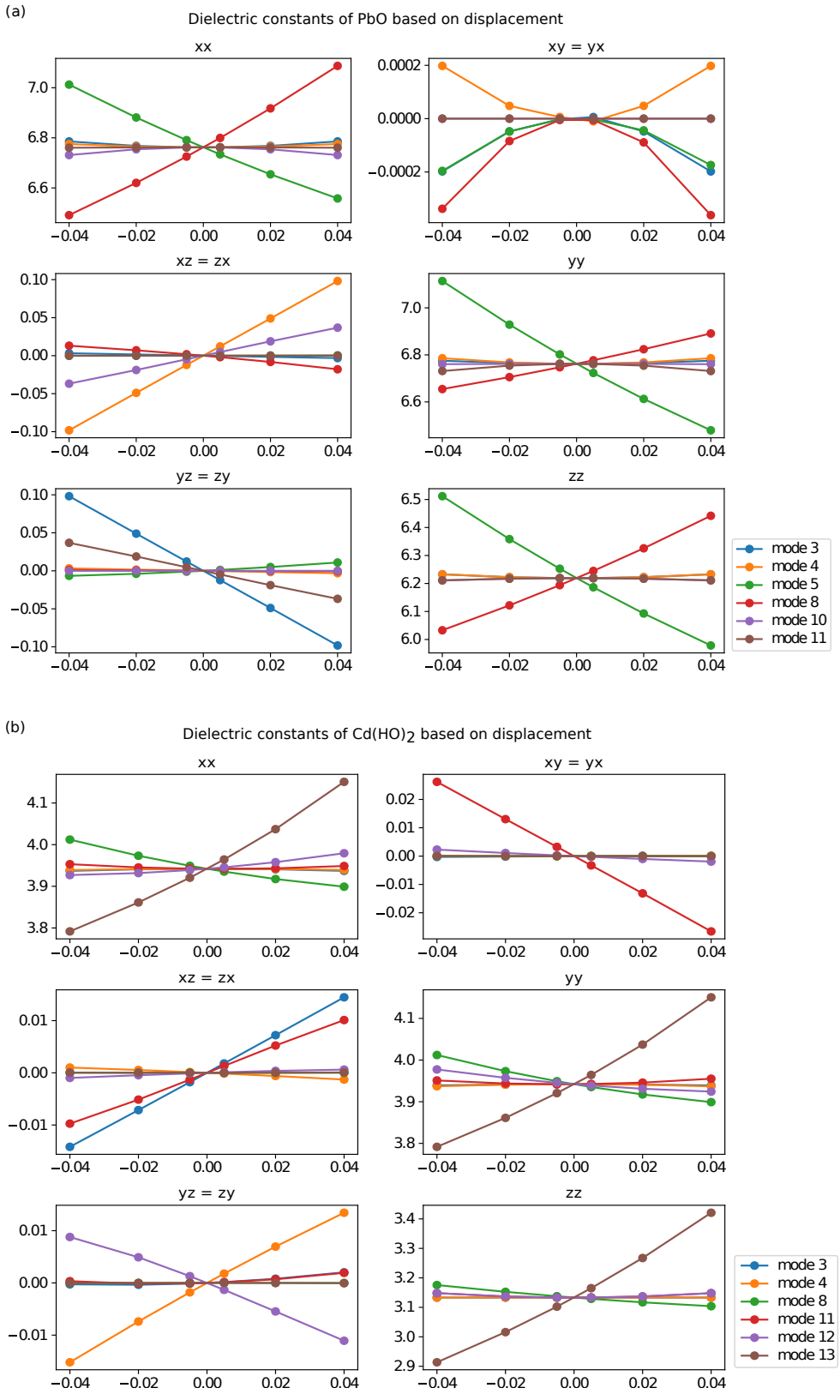

Figure S2. Changes of dielectric constant of (a) PbO and (b) $Cd(HO)_2$ in different directions as a function of the displacement step size (0.005–0.04).

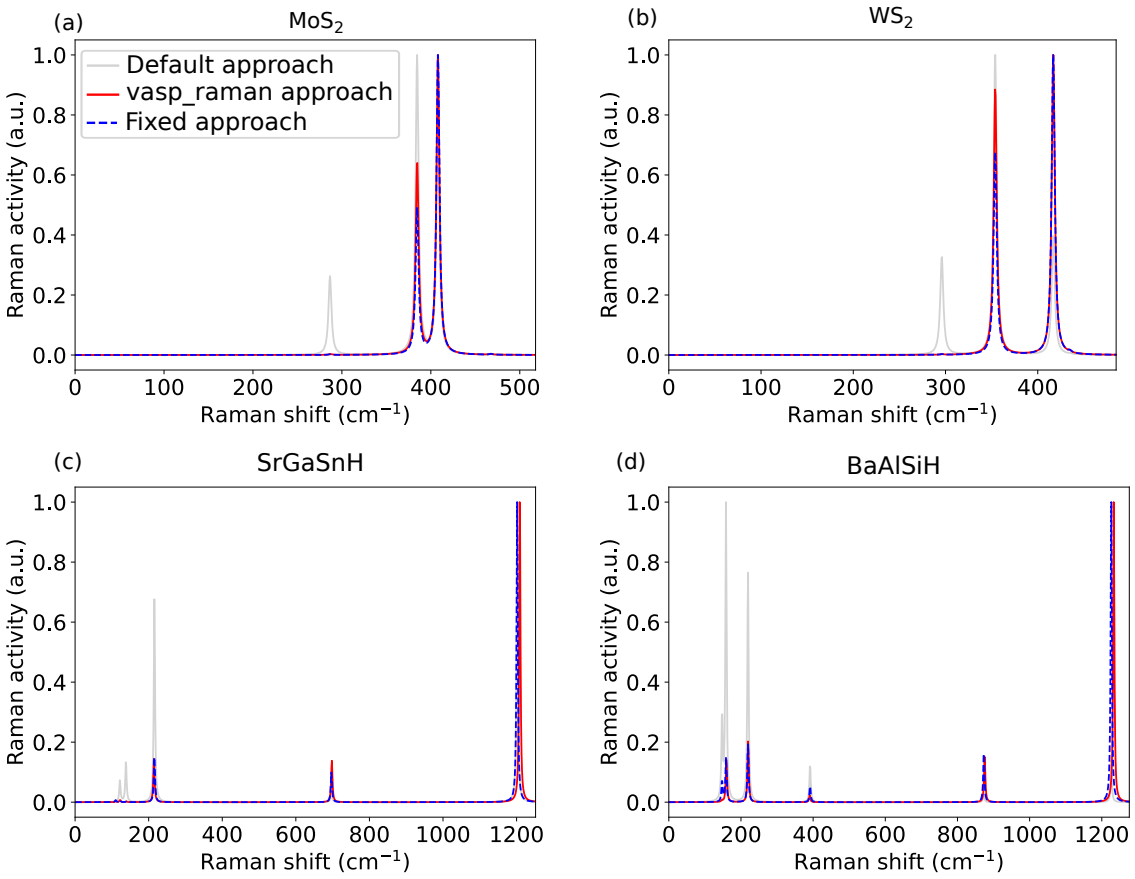

Figure S3. Comparison of the Raman activity from our workflow and that from vasp_raman code. The spectra from old version of Atomate with incorrect eigenvector normalization is also shown.

References

1. Fonari, A. & Stauffer, S. Source code for: Python program to evaluate off-resonance raman activity using vasp code as the backend. *Github* https://github.com/raman-sc/VASP/ (2013).
2. Porezag, D. & Pederson, M. R. Infrared intensities and Raman-scattering activities within density-functional theory. *Phys. Rev. B - Condens. Matter Mater. Phys.* **54**, 7830–7836, https://doi.org/10.1103/PhysRevB.54.7830 (1996).
3. Prosandeev, S. A., Waghmare, U., Levin, I. & Maslar, J. First-order Raman spectra of $AB'_{1/2}B''_{1/2}O_3$ double perovskites. *Phys. Rev. B - Condens. Matter Mater. Phys.* **71**, 1–9, https://doi.org/10.1103/PhysRevB.71.214307 (2005).
4. Long, D. A. *The Raman effect* (John Wiley & Sons, Chichester, England, 2002).